

Ground-state electronic properties of diamond in the local-density formalism*

Alex Zunger and A. J. Freeman

Physics Department and Materials Research Center, Northwestern University, Evanston, Illinois 60201

(Received 26 August 1976)

We use our previously reported method for solving self-consistently the local-density one-particle equations in a numerical-basis-set linear combination of atomic orbitals expansion to study the ground-state charge density, x-ray structure factors, directional Compton profile, total energy, cohesive energy, equilibrium lattice constant, and behavior of one-electron properties under pressure of diamond. Good agreement is obtained with available experiment data. The results are compared with those obtained by the restricted Hartree-Fock model: the role of electron exchange and correlation on the binding mechanism, the charge density, and the momentum density is discussed.

I. INTRODUCTION

The local density functional (LDF) formalism of Hohenberg, Kohn, and Sham,^{1,2} and its recent extension as a local spin-density functional formalism,³ form the basis of a new approach to the study of electronic structure in that the effects of exchange and correlation are incorporated directly into a charge-density-dependent potential term that is determined self-consistently from the solution of an effective one-particle equation. Applications of the LDF formalism to atoms^{4,5} and molecules⁶ have yielded encouraging results. Similar applications for solids are complicated by (i) the need to consider both the short-range and the long-range multicenter crystal potential having nonspherical components, (ii) the difficulties in obtaining full self-consistency in a periodic system, and (iii) the need to provide a basis set with sufficient variational flexibility. Hence, theoretical studies of ground-state electronic properties of solids in the LDF formalism have been mainly limited to muffin-tin models for the potential,^{7,8} non-self-consistent schemes,⁹ treatments of simplified jellium models¹⁰ or spherical cellular schemes.^{11,12}

We have recently proposed^{13,14} a general self-consistent method for solving the LDF formalism one-particle equation for realistic solids using a numerical-basis-set LCAO (linear combination of atomic orbitals) expansion and retaining all nonspherical parts of the crystal potential. We have demonstrated a rapid convergence of the self-consistent (SC) cycle when the treatment of the full crystal charge density is suitably apportioned between real-space and Fourier-transformed reciprocal-space parts and have indicated the large degree of variational flexibility offered by a nonlinearly optimized (exact) numerical atomic-like basis set. We have shown that all multicenter interactions as well as the nonconstant parts of the crystal potential are efficiently treated by

a three-dimensional Diophantine integration scheme.

The purpose of this paper is to illustrate the applicability of our method to real systems by studying the ground-state electronic properties of diamond. Diamond has been long considered as a prototype for covalently bonded insulators¹⁵ and a great deal of experimental work has been done on its ground-state properties, including cohesive energy,¹⁶ lattice-constant studies,¹⁷ x-ray scattering factors,^{18,19} charge density,¹⁸ and directional Compton profile.^{20,21} In addition, theoretical studies on its ground-state properties within the restricted Hartree-Fock (RHF) model are available²²⁻²⁵ so comparison with the predictions of the LDF formalism is possible. Although the *eigenvalue spectrum* (band structure) of the local exchange Hamiltonian for diamond has been studied previously by a variety of first-principles techniques [augmented planes waves (APW),^{26,27} orthogonalized plane waves (OPW),²⁸⁻³⁰ pseudo-potential OPW,³¹ LCAO,³²⁻³⁵ and cellular methods¹¹], the ground-state observables related to the ground-state crystal charge density have received much less attention. While our method was shown¹³ to accurately reproduce the band structure of diamond as obtained by other techniques^{32,33} (when correlation and self-consistency is omitted so as to be compatible with the previously published band-structure models and the full nonspherical components of the potential are retained in both calculations), we do not consider this as a stringent test since the LDF formalism in its "standard" form does not make any claim on the physical significance of the band eigenvalues nor are these eigenvalues sensitive enough to the details of the basis set and potential.³⁶ In what follows we present our results for the x-ray scattering factors, charge density, directional Compton profile, total energy, and equilibrium lattice constant and discuss the role of exchange

and correlation in determining these observables. Comparisons are made with earlier Hartree-Fock results²²⁻²⁵ and with experiment.

II. METHOD OF CALCULATION

Since the method was described at length elsewhere,¹³ we give only a brief description here in order to place our work in proper perspective. Basically, our aim is to solve the effective one-particle equation in the local density functional formalism, i.e., the Bloch equation in which the potential consists of a Coulomb and an exchange and correlation potential $V_{xc}(\rho(\vec{r}))$ which is given as a functional derivative of the total exchange and correlation energy $E_{xc}(\rho(\vec{r}))$ of an interacting (inhomogeneous) electron gas with respect to the charge density.¹ In our work, we use only the free-electron exchange and correlation potential

terms^{1,2} which are the first two terms in a general expansion^{1,37} of $E_{xc}(\rho(\vec{r}))$. For the free-electron correlation term we use the results of Singwi *et al.*³⁸ as fitted to an analytic form.³⁹

One writes the ground-state charge density $\rho(\vec{r})$ as

$$\rho(\vec{r}) = \frac{N\Omega}{(2\pi)^3} \sum_{j=1}^{\sigma_{oc}} \int_{BZ} n_j(\vec{k}) \times \psi_j^*(\vec{k}, \vec{r}) \psi_j(\vec{k}, \vec{r}) d\vec{k}, \quad (1)$$

where $n_j(\vec{k})$ is the Fermi occupation number of the σ_{oc} occupied crystal eigenfunctions $\psi_j(\vec{k}, \vec{r})$ of band j and wave vector \vec{k} ; and N and Ω denote the number of unit cells and the unit cell volume, respectively. The integration is performed over the occupied part of the Brillouin zone (BZ). The total ground-state energy is given by

$$E_{tot} = \sum_{j,k} n_j(\vec{k}) \langle \psi_j(\vec{k}, \vec{r}) | -\frac{1}{2} \nabla^2 | \psi_j(\vec{k}, \vec{r}) \rangle + \int \rho(\vec{r}) \left(\sum_{m,\alpha} \frac{-Z_\alpha}{|\vec{r} - \vec{R}_m - \vec{d}_\alpha|} + \frac{1}{2} \int \frac{\rho(\vec{r}')}{|\vec{r} - \vec{r}'|} d\vec{r}' \right) d\vec{r} + \sum_{\substack{m\alpha, n\beta \\ m\alpha \neq n\beta}} \frac{Z_\alpha Z_\beta}{|\vec{R}_m + \vec{d}_\alpha - \vec{R}_n - \vec{d}_\beta|} + E_{xc}(\rho(\vec{r})), \quad (2)$$

where Z_α is the nuclear charge of the atom situated at site \vec{d}_α and \vec{R}_m denotes the position vector of the m th unit cell.

It is clear that, because of the functional dependence of the potentials on $\rho(\vec{r})$ and hence on the wave functions $\{\psi_j(\vec{k}, \vec{r})\}$, the solutions must be obtained by some self-consistent (SC) procedure. As our initial guess for the crystal density (which will be subsequently refined in the SC iterative cycle) we chose a population-dependent overlapping atomic densities model

$$\rho^{sup}(\vec{r}) = \sum_m^N \sum_\alpha^h \rho_\alpha(\vec{r} - \vec{R}_m - \vec{d}_\alpha, \{f_{n'l}^\alpha, Q^\alpha\}), \quad (3)$$

where $\rho_\alpha(\vec{r}, \{f_{n'l}^\alpha, Q^\alpha\})$ is the charge density of atom (ion) α calculated numerically from an atomic (ionic) LDF one-particle equation assuming occupation numbers $f_{n'l}^\alpha$, for the central-field quantum numbers $n'l'$ and a possible net ionic charge Q^α . In solving these equation we use the same functional form of $V_{xc}(\rho_\alpha(\vec{r}))$ as used for the crystal case but replace the crystal density with $\rho_\alpha(\vec{r})$. The atomic eigenfunctions $\varphi_{n'l}^\alpha(\vec{r})$ are used to determine (self-consistently) the one-site density by

$$\rho_\alpha(r, \{f_{n'l}^\alpha, Q^\alpha\}) = \sum_{n'l} f_{n'l}^\alpha \varphi_{n'l}^{\alpha*}(r) \varphi_{n'l}(r), \quad (4)$$

and because of the assumed spherical symmetry these are easily solved for self-consistently in numerical form for an assumed set of atomic popu-

lations and charge $\{f_{n'l}^\alpha, Q^\alpha\}$ (a typical accuracy of 10^{-5} a.u. is obtained for the eigenvalues). The superposition density is then formed by carrying the sum in Eq. (3) to convergence (a summation radius of 20 a.u. is employed). The initial guess for the crystal potential is obtained by solving Poisson's equation for $\rho^{sup}(\vec{r})$ and using the exchange and correlation functionals with this model density. The Coulomb superposition potential is separated into short-range $V_{SRC}^{sup}(\vec{r})$ and a long-range $V_{LRC}^{sup}(\vec{r})$ parts. The first is simply given by a direct lattice sum of the short-range (overlapping) ionic potential

$$V_{SRC}^{sup}(\vec{r}) = \sum_m^{R_{max}} \sum_\alpha \left(V_\alpha(\vec{r} - \vec{R}_m - \vec{d}_\alpha) + \frac{Q^\alpha}{|\vec{r} - \vec{R}_m - \vec{d}_\alpha|} \right), \quad (5)$$

where the quantity in large parentheses denotes the Coulomb potential associated with the neutralized charge of site α . This sum converges rapidly due to the subtraction of the long-range ionic tails in Eq. (5) and a summation radius of $R_{max} \approx 17-22$ a.u. is sufficient to achieve an accuracy of $10^{-4}-10^{-6}$ a.u. The remaining long-range Coulomb term is calculated by the Ewald⁴⁰ technique using the effective charges

$$Q^\alpha = \lim_{r \rightarrow R_{max}} r V_\alpha(r).$$

The exchange and correlation "superposition" potentials are given by applying the respective func-

tionals to $\rho^{\text{sup}}(\vec{r})$ (i.e., without linearizing these potentials with respect to the individual^{28,35} ρ_α 's). Note that all aspherical contributions originating from the overlapping tails of the one-site density $\rho_\alpha(r)$, as well as those contributed by the point-ion electrostatic crystal field, are fully retained. However, owing to the nonlinearity of the exchange and correlation functionals with respect to the individual single-site densities $\rho_\alpha(r)$, the initial superposition potential $V^{\text{sup}}(\vec{r})$ is not representable as a lattice sum of one-center terms and hence even at this zeroth iteration stage the one-particle equation constitutes a multicenter problem. After convergence of the direct lattice sums [Eqs. (3) and (5)] is obtained, $V^{\text{sup}}(\vec{r})$ is completely defined by specifying the atomic numbers Z_α , the postulated crystal structure and the assumed populations and charges $\{f_{nI}^\alpha, Q^\alpha\}$. The latter are subsequently used as free parameters in the SC procedure to optimize the superposition potential (see below). By changing the relative proportions (i.e., hybridization ratio) of the populations in the atomic LDF equations (e.g., the carbon 2s to 2p populations) the superposition density and potential can be made to better simulate the output crystal density and potential so as to facilitate the convergence of the SC cycle.

The crystal wave functions $\psi_j(\vec{k}, \vec{r})$ are expanded in terms of $h\eta$ Bloch functions $\Phi_{\mu\alpha}(\vec{k}, \vec{r})$ in standard form:

$$\psi_j(\vec{k}, \vec{r}) = \sum_{\alpha=1}^h \sum_{\mu=1}^{\eta} C_{\mu\alpha j}(\vec{k}) \Phi_{\mu\alpha}(\vec{k}, \vec{r}), \quad (6)$$

where $\Phi_{\mu\alpha}(\vec{k}, \vec{r})$ is defined in terms of the μ th basis orbital $\chi_\mu^\alpha(\vec{r})$ situated on the α th site:

$$\Phi_{\mu\alpha}(\vec{k}, \vec{r}) = N^{-1/2} \sum_m e^{i\vec{k}\cdot\vec{R}_m} \chi_\mu^\alpha(\vec{r} - \vec{d}_\alpha - \vec{R}_m). \quad (7)$$

We use as LCAO basis functions *numerical* atomic-like LDF orbitals. These are obtained from a solution of an atomlike equation, similar to that used to generate the superposition potential

$$\begin{aligned} & \left[-\frac{1}{2} \nabla^2 + g_\alpha(r) \right] \chi_{nI}^\alpha(r, \{f_{nI}^\alpha, Q^\alpha\}) \\ & = \epsilon_{nI} \chi_{nI}^\alpha(r, \{f_{nI}^\alpha, Q^\alpha\}). \end{aligned} \quad (8)$$

Here, the one-site potential $g_\alpha(r)$ can be taken as a generalized atomlike potential as long as it generates through Eq. (8) orbitals that form an accurate and rapidly convergent basis set for expanding the crystal orbitals $\psi_j(\vec{k}, \vec{r})$. Such basis orbitals have to maintain the correct cusps near the nuclei (which are absent in a Gaussian basis) as well as appropriate nodal behavior and angular variation, while any long-range tail is unwarranted (due to the possibility of formation of linear dependence between the Bloch functions). We hence

chose $g_\alpha(r)$ in Eq. (8) to be the usual atomic potential plus an additional external potential $A(r)$ in a form of a potential well starting from a distance R_c from the nucleus. This distance is chosen so that the low-lying occupied solutions of Eq. (8) will be identical with the exact atomic solution, while the virtual orbitals (3s, 3p, and 3d in carbon) will have compressed tails. Experimentation with this type of localizing potential¹³ revealed that it is rather straightforward to chose R_c (e.g., 17 a.u. for carbon) so that the resulting orbitals will be sufficiently localized so as to enhance the Bloch sums convergence [Eq. (7)] and still possess sufficient variational quality in the crystal calculation (e.g., produce a total energy that is as low as that obtained with regular atomic orbitals). The basis set obtained in this way (for a fixed choice of $\{f_{nI}^\alpha, Q^\alpha\}$) is used to our work in direct tabular form with no attempt to fit it to an analytic set. Extensive studies of the basis-set problem¹³ (i.e., addition of analytic Slater orbitals to a minimal basis set to better span the virtual space) have shown that a numerical basis set for carbon consisting of 1s, 2s, 2p, 3s, 3p orbitals (18 orbitals per unit cell denoted here as set I) is sufficient to maintain an accuracy of about 3 mRy in the valence and lowest two conduction-band eigenvalues for diamond. In the calculation of the *total* crystal energy it was found that the convergence of the result due to additional virtual numerical (or Slater) orbitals was rather slow but that augmenting the basis set by ion-pair charge-transfer orbitals [i.e., solving Eq. (8) for a neutral carbon atom with $Q^\alpha = 0$ as well as for $Q^\alpha = 0.8$ and $Q^\alpha = -0.8$ and using this triple-sized set for the crystal] produced a substantial improvement in the result. We hence use this extended set (denoted here as set II) in this work to calculate total energies and equilibrium lattice constants and compare the results with the more economic set I.

Having defined the initial crystal potential and the basis set, the usual linear variation secular equation is given as

$$\sum_{\mu}^{\eta} \sum_{\alpha}^h [H_{\mu\alpha, \nu\beta}(\vec{k}) - S_{\mu\alpha\nu\beta}(\vec{k}) \epsilon_j(\vec{k})] C_{\mu\alpha j}(\vec{k}) = 0, \quad (9)$$

where the Hamiltonian and overlap matrix elements in the Bloch representation are

$$H_{\mu\alpha, \nu\beta}(\vec{k}) = \langle \Phi_{\mu\alpha}(\vec{k}, \vec{r}) | -\frac{1}{2} \nabla^2 + V(\vec{r}) | \Phi_{\nu\beta}(\vec{k}, \vec{r}) \rangle, \quad (10a)$$

$$S_{\mu\alpha, \nu\beta}(\vec{k}) = \langle \Phi_{\mu\alpha}(\vec{k}, \vec{r}) | \Phi_{\nu\beta}(\vec{k}, \vec{r}) \rangle. \quad (10b)$$

These matrix elements, when expanded in terms of the basis orbitals $\chi_\mu^\alpha(r)$ and the projected single-site potentials, give rise to a large number of two-

and three-center integrals. The computational difficulty in handling these integrations has led many workers in both molecular and solid-state electronic structure theory to resort to somewhat artificial analytic basis functions (e.g., Gaussians) or to simply neglect a large number of these integrals. In the present work, we resolve that problem by evaluating the integrals directly from Eq. (10) (using numerical forms for the potential and Bloch functions) employing a three-dimensional Diophantine integration scheme.⁴¹ The details of the application of this scheme are given elsewhere.^{13,32} Here we only note that in using this approach all the multicenter integrals are avoided and that any general form for the potential (various forms for correlation, non-muffin-tin corrections, etc.) or basis functions can be treated equally in a direct manner. The use of an exact numerical basis set along with a superposition potential generated from the same set $\{f_{n_i}, Q^\alpha\}$ offers another advantage¹³: the integrand appearing in Eq. (10a) exhibits an algebraic cancellation between the repulsive kinetic energy and the attractive Coulomb singularity in the vicinity of the nuclei in the solid so that the Hamiltonian elements can be calculated to good accuracy. About 2000 Diophantine integration points are required to obtain an accuracy of 2 mRy in the valence and first two conduction-band eigenvalues in diamond while some 7000 points are required for an accuracy of 0.2 eV in the total energy calculation.

The secular equation [Eq. (9)] is solved at a set of reciprocal-lattice vectors \vec{k}_i ; $i = 1, \dots, p_i$. The resulting eigenfunctions are used to construct a refined crystal density $\rho_{\text{cry}}(\vec{r})$ from Eq. (1) where the integration over the BZ is replaced by a summation over the p_i wave vectors $\{\vec{k}_i\}$. We chose, for the set $\{\vec{k}_i\}$, the first 10 (inequivalent) special \vec{k} points in the diamond BZ and their associated weights.⁴² We note that due to the low dispersion of $\psi_j^*(\vec{k}, \vec{r})\psi_j(\vec{k}, \vec{r})$ in diamond across the BZ¹³ this approximation to the charge density does not cause any severe problems in calculating $\rho_{\text{cry}}(\vec{r})$ and the total energy; however, the calculation of the BZ average of the *band eigenvalues* (needed for the calculation of the kinetic energy term) requires more \vec{k} points due to the substantial width of the valence band and is calculated in the present study by averaging 32 inequivalent \vec{k} points.

Given the output crystal density, we set a self-consistent cycle that is based on two stages. In stage 1 (charge and configuration self-consistency), we iterate over the population numbers $\{f_{n_i}^\alpha\}$ and charge Q^α , solving at each stage for a new superposition potential and numerical basis orbitals [Eq. (8)] so as to minimize in the least-squares sense the deviation $\Delta\rho(\vec{r})$ between the crystal den-

sity $\rho_{\text{cry}}(\vec{r})$ and the population-dependent superposition density $\rho^{\text{sup}}(\vec{r})$. During these iterations electronic charge is redistributed from the occupied atomic orbitals to the formerly virtual orbitals resulting in a radial distortion of the basis set. We thus allow our basis set to relax to the current form of the iterated crystal potential by varying it *nonlinearly*. In carrying stage 1 in SC to completion, the residual function $\Delta\rho(\vec{r})$ is minimized over space and most of its localized features (present at the first iteration) are smoothed out. In other words, by varying simultaneously the basis set (allowing for radial distortion, shift of nodes, and rehybridization) and crystal potential, we select among all possible superposition densities the one that best simulates the actual crystal potential. This procedure requires about 4–5 iterations in diamond. The residual density $\Delta\rho(\vec{r})$ obtained at the end of this stage represents the “misplaced” charge that is not amenable to a superposition representation using one-center terms located on existing atomic sites. It turns out that due to the substantial penetration of charge from nearest neighbors into the inner region of the central atom, the full site anisotropy in diamond could not be satisfactorily represented by an optimized superposition model (a standard deviation of $0.09e$ is obtained). The inclusion of the residual $\Delta\rho(\vec{r})$ is done in stage 2 of SC (“full SC”) by Fourier transforming numerically the residual charge

$$\Delta\rho(\vec{K}_s) = \frac{1}{\Omega} \int_{\text{uc}} e^{-i\vec{K}_s \cdot \vec{r}} \Delta\rho(\vec{r}) d\vec{r}, \quad (11)$$

(the integration over the unit cell being performed by the Diophantine method) and calculating the change in the electronic Coulomb potential due to this density using a direct Fourier series

$$\Delta V_{\text{Coul}}(\vec{r}) = \sum_{\vec{K}_s \neq 0} 4\pi \frac{\Delta\rho(\vec{K}_s)}{|\vec{K}_s|^2} e^{i\vec{K}_s \cdot \vec{r}}. \quad (12)$$

This change in the Coulomb potential is added to $V_{\text{SRC}}^{\text{sup}}(\vec{r}) + V_{\text{LRC}}^{\text{sup}}(\vec{r})$ obtained in the last charge and configuration SC iteration. The iterated exchange and correlation potential is computed using the full density $\rho_{\text{cry}}(\vec{r})$ and the solution of the eigenvalue problem [Eq. (9)] is repeated iteratively so as to diminish $\Delta\rho(\vec{r})$. Owing to the absorption of the corelike cusps and localized features into $\rho^{\text{sup}}(\vec{r})$ in stage 1 in SC, the Fourier series in Eq. (12) converges rapidly (only the first seven stars are needed) and only 3–4 iterations are required. It is noted that in performing full self-consistency we go considerably beyond the “standard” degrees of self-consistency obtained in either muffin-tin-type treatments⁴³ (in which the iterated redistributed charge density is spherically averaged before

the next iteration is attempted) or conventional local-density LCAO schemes (in which only charge and configuration SC is maintained using either Mulliken populations⁴⁴ or spherical Gaussians⁴⁵ as a superposition projection set). In what follows we will discuss the results of the treatment described above for the ground state electronic properties of diamond using our final fully self-consistent results.

III. RESULTS AND DISCUSSION

A. Charge density and x-ray scattering factors

In order to examine the effects of exchange and correlation on the ground-state charge density in diamond we have performed three fully self-consistent calculations; the first employed only the electrostatic electron-electron and electron-nuclear potential in the one-particle equation ("electrostatic model"), the second incorporated also the local exchange ("exchange model"), while in the third calculation the correlation potential was also considered ("exchange and correlation model"). All three calculations used an extended numerical set (1s, 2s, 2p, 3s, and 3p orbitals per carbon) and all lattice sums were performed to convergence. The lattice constant was fixed at 6.740 a.u. We arbitrarily define "exchange charge" as the total valence (i.e., the two lowest 1s bands are omitted) ground-state charge-density difference between the exchange and the electrostatic models while the "correlation charge" is defined as the corresponding density difference between the exchange and correlation model and the exchange model. Figures 1 and 2 show the contribution of some high-symmetry states in the BZ to the exchange and correlation charge density, respectively, along the [111] bond direction in diamond and Fig. 3 shows the corresponding charge-density contributions to the total valence charge density. Figure 4 compares the correlation charge along two directions in the crystal.

The main conclusions to be drawn from these comparisons are the following:

- (i) The exchange charge density alters the electrostatic charge density by as much as (10-40)% in the region around the center of the bond while the correlation charge density is responsible for only a (0.1-0.3)% change. The exchange charge is about two orders of magnitude larger than the correlation in most of the bond region.
- (ii) Both the exchange and correlation charge densities show substantial \vec{k} -space dispersion. The relative changes in various \vec{k} -space contributions are larger than the corresponding variations in the contributions to the total valence density. The

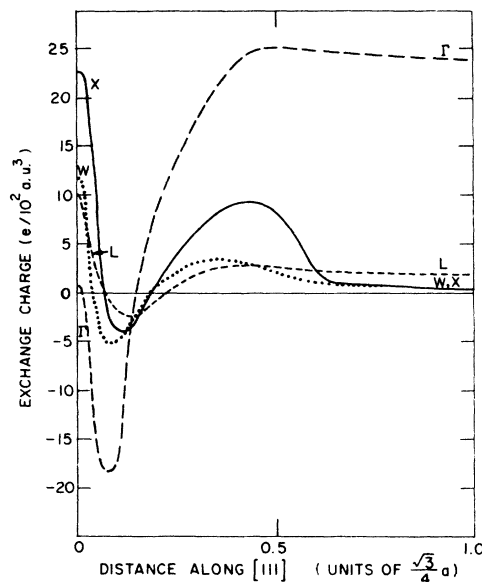


FIG. 1. Contributions of some high-symmetry states in the BZ to the valence "exchange charge density" in diamond along the [111] direction. The two lowest 1s-like bands are not included. The density difference shown results from two independent exchange-model and electrostatic-model calculations. A carbon atom is located at the origin while the right side of the x axis corresponds to the center of the C-C bond.

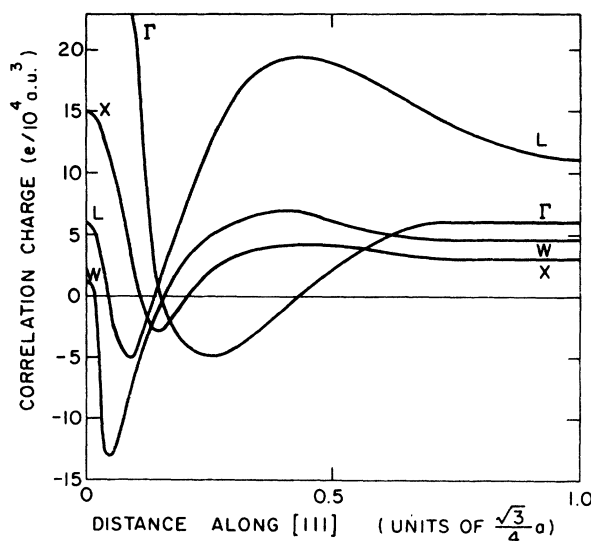


FIG. 2. Contribution of some high-symmetry states in the BZ to the valence "correlation charge density" in diamond along the [111] direction. The two lowest 1s-like bands are not included. A carbon atom is located at the origin while the right-hand side of the x axis corresponds to the center of the C-C bond.

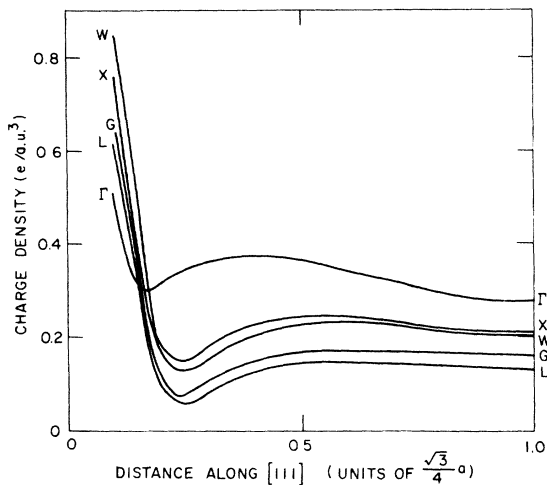


FIG. 3. Ground-state valence charge density in diamond along the [111] direction. Γ , X, L, and W are the high-symmetry points while G denotes a general point. A carbon atom is at the origin while the right-hand side of the x axis corresponds to the center of the C-C bond.

full valence density (Fig. 3) generally shows a rather low \vec{k} -space dispersion (compare contributions at X, W, and L to that of the randomly chosen general point G). The Γ point is an exception owing to its high symmetry. The directional anisotropy of the exchange and correlation charges in real space is quite small.

(iii) The over-all effect of both exchange and correlation on the charge density is to enhance the charge buildup around the center of the bond and to substantially increase the charge localization on the atoms, at the expense of deleting some charge density from a doughnut-shaped region at

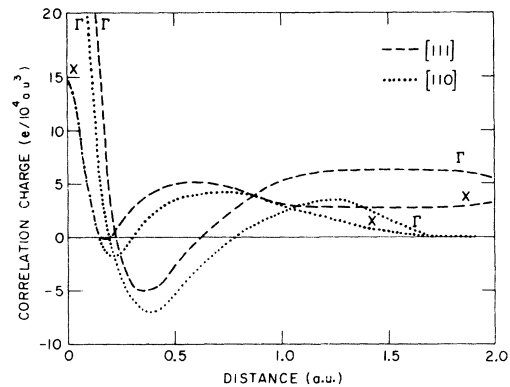


FIG. 4. Contributions of the X and Γ points to the valence correlation charge in diamond along the [111] and [110] directions.

about 0.2–0.4 a.u. from each atom. A similar localization and sharpening of charge density close to the atomic site due to the incorporation of the correlation functional in the potential was also observed in a separate calculation on an isolated carbon atom (e.g., some 2% decrease in $\langle r^2 \rangle$). The observed effect in the solid is however much more pronounced (volume effects being taken into account) indicating an additional charge localization mechanism in the solid near the cores *due to the enhancement of the overlap of wave functions from neighboring sites*. It thus seems that the charge-density changes introduced by exchange and correlation, both close to the nuclei and around the bond center, act to increase the stability of the solid relative to the noninteracting atoms.

Table I shows the calculated x-ray scattering

TABLE I. Calculated and experimental x-ray scattering factors for diamond

$$f(\vec{K}_s) = \frac{1}{\Omega} \int \exp(i\vec{K}_s \cdot \vec{r}) \rho_{\text{cry}}(\vec{r}) d\vec{r}.$$

$f(0,0,0)$ equals 6.0. The "superposition model" results are calculated in the exchange model assuming the $1s^2 2s^2 2p^2$ configuration for the atoms and a charge density given in Eq. (3).

| hkl | Electrostatic model | Exchange model | Exchange and correlation model | Expt. ^a | Hartree Fock ^c | Superposition model |
|-------|---------------------|----------------|--------------------------------|--------------------|---------------------------|---------------------|
| 111 | 3.062 | 3.273 | 3.281 | 3.32 | 3.29 | 3.005 |
| 220 | 1.936 | 1.992 | 1.995 | 1.98 | 1.93 | 1.964 |
| 311 | 1.656 | 1.720 | 1.692 | 1.66 | 1.69 | 1.760 |
| 222 | 0.066 | 0.137 | 0.139 | 0.144 ^b | 0.08 | 0.0 |
| 400 | 1.470 | 1.494 | 1.493 | 1.48 | 1.57 | 1.585 |
| 331 | 1.625 | 1.600 | 1.605 | 1.58 | 1.55 | 1.519 |
| 422 | 1.411 | 1.423 | 1.408 | 1.42 | 1.42 | 1.432 |
| 511 | 1.347 | 1.385 | 1.392 | 1.42 | ... | 1.387 |
| 333 | 1.346 | 1.381 | 1.392 | 1.42 | ... | 1.387 |

^a Reference 18.

^b Reference 19.

^c References 22 and 25.

factors in diamond at the three levels of local density approximations, together with the experimental results^{18,19} and the canonical Hartree-Fock results of Euwema *et al.* obtained using an *s* and *p* Gaussian basis set.^{22,25} It is apparent that exchange acts to increase the low-angle scattering factors quite dramatically, reflecting the increased localization of charge in the interatomic region, with the correlation effect being much smaller. In particular, the calculated (222) forbidden reflection (forbidden in the approximation in which the charge density is given as a superposition of spherically symmetric, possibly overlapping, atomic densities, last column in Table I) is increased by about a factor of 2 upon introducing exchange in the potential. The value of this scattering factor turned out to be particularly sensitive to the details of the self-consistency maintained in the calculation and to the quality of the basis set⁴⁷ (e.g., a minimal basis set yielded a value of 0.082 while a non-self-consistent extended basis set yielded a value of 0.089). We note from Table I that a band model that allows for *wave-function* overlap produces markedly improved results over a spherical superposition model (last column).

The general agreement between our calculated results and experiment is reasonable. It is apparent from the comparison of the atomic and crystal values that, as expected, the scattering factors constitute a sensitive test of the details of the calculated charge density only for the first few reflections to which the density in the outer regions of the cell contribute. Similar conclusions can be drawn from comparing our exchange-model results with those obtained in the literature⁴⁸⁻⁵² by a number of approximations to the local exchange

problem (Table II). Although these calculations employ various independent approximations, the results vary only in the first few reflections.

B. Self-consistent crystal potential and the band structure

We next consider the contributions of exchange and correlation to the self-consistent crystal potential. Figure 5 shows the components of the final SC crystal potential, as obtained in the exchange model and in the exchange and correlation model, respectively, along the bond direction in diamond. It is observed that the exchange and correlation potentials constitute some 50 and 5% of the electrostatic crystal potential at the bond center with their relative contribution to the total potential decreasing rapidly as one moves towards the atomic sites. To further elucidate the role of exchange and correlation in the Hamiltonian matrix representation, we show in Fig. 6 the spatial behavior of some typical Bloch functions at the Γ point acted on by the kinetic-energy operator and by the SC exchange potential operator. It is seen that the function $V_x(\vec{r})\Phi_\mu^\alpha(0, \vec{r})$ is largely cancelled near the core region due to the steep kinetic-energy contributions and it is only in the bond region that the exchange potential contributes significantly to the Hamiltonian matrix elements. The same conclusion is also valid for the correlation potential which has rather small and finite values in the core region. Thus it is the bond region where the exchange and correlation potential are expected to be important.⁵³ When the potential is computed along the [110], [111], and [100] directions in the crystal, it is observed the electrostatic, exchange, and correlation potential exhibit maximum anisotropies of 42%, 48%, and 32%

TABLE II. Comparison of several model calculations of the x-ray scattering factors in diamond.

| <i>hkl</i> | SC OPW ^a | Pseudopotential <i>t</i> matrix ^b | Pseudopotential OPW ^c | Equivalent orbitals ^d | Present study |
|------------|---------------------|--|----------------------------------|----------------------------------|---------------|
| 111 | 3.23 | 3.21 | 3.32 | 3.31 | 3.27 |
| 220 | 1.92 | 1.91 | 1.97 | 1.94 | 1.99 |
| 311 | 1.64 | 1.58 | 1.66 | 1.69 | 1.72 |
| 222 | 0.12 | 0.13 | 0.15 | 0.064 | 0.137 |
| 400 | 1.52 | 1.51 | 1.48 | 1.57 | 1.49 |
| 331 | 1.52 | ... | ... | 1.54 | 1.60 |
| 422 | 1.40 | ... | ... | ... | 1.42 |
| 511 | 1.35 | ... | ... | ... | 1.38 |
| 333 | 1.32 | ... | ... | ... | 1.38 |

^a Self-consistent OPW calculation, Ref. 48, for an exchange coefficient of $\frac{2}{3}$.

^b Reference 49.

^c References 50 and 51.

^d Reference 52.

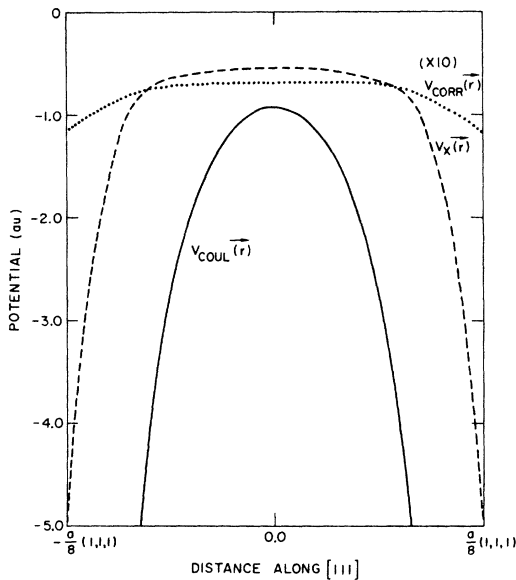


FIG. 5. Self-consistent crystal potential in diamond along the [111] direction. $V_{\text{COUL}}(\vec{r})$, $V_X(\vec{r})$, and $V_{\text{CORR}}(\vec{r})$ denote the Coulomb, exchange and correlation potentials, respectively.

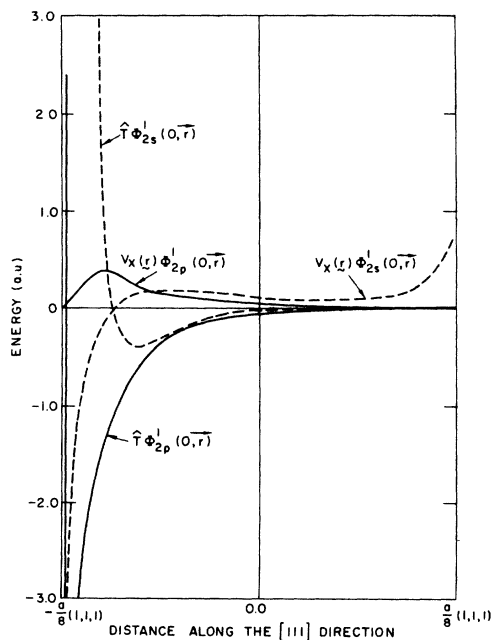


FIG. 6. Spatial behavior of the self-consistent exchange potential acting on a Bloch function (at Γ) $V_X(\vec{r})\Phi_\mu^1(0, \vec{r})$ and the kinetic energy associated with this Bloch state $T\Phi_\mu^1(0, \vec{r})$, along the [111] direction. Results corresponding to $\mu=2s, 2p$ and to the Bloch states belonging to sublattice 1 [at $-\frac{1}{8}a(1,1,1)$] are shown.

respectively, relative to their average values at a constant distant from the bond center. One would thus conclude that the full anisotropy (non-muffin-tin corrections) of the electrostatic and exchange potentials should be carefully treated in the valence region in covalent system.^{26, 27}

The eigenvalue spectrum obtained at the end of the SC exchange and correlation calculation is depicted in Fig. 7. The general shape of the dispersion curves is generally similar to that obtained in the past with different exchange models.^{32, 33} The minimum in the first unoccupied band occurs at $(0.77, 0, 0)$. For comparison with other results we give in Table III the actual eigenvalues obtained at some high-symmetry points in the BZ. Upon removing the correlation potential from the calculation the eigenvalue spectra moves almost rigidly upwards, by about 0.7 eV. The difference in *relative* eigenvalues between the exchange and the exchange and correlation models is less than 0.05 eV over the entire occupied volume of the BZ. It thus appears that aside from an almost constant shift, the band structure is rather insensitive to the correlation potential and that it could probably be completely ignored in a conventional band calculation. On the other hand, as expected, the Hartree-type electrostatic model predicts a radically different eigenvalue spectrum; the lowest unoccupied bands move down by some 6 eV while the top of the valence band is lowered by about 2.5 eV resulting in a net de-

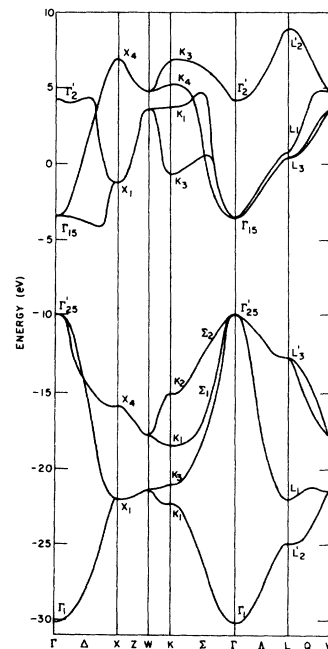


FIG. 7. Self-consistent exchange and correlation band structure for diamond.

crease of the direct gap by 3.5 eV. The bottom of the valence band changes by less than 0.2 eV. The effects of the removal of the exchange potential are manifested mainly on the states above the lowest valence band, again reflecting the relative insensitivity of the regions near the atomic cores to the exchange potential. We note that although the one-particle energies of the occupied states are stabilized by removal of the exchange potential, the *total* crystal energy is destabilized (i.e., it is less attractive) on account of the reduced charge buildup in the bond region and the diminished charge localization at the atomic sites (compare Fig. 1). This is in direct contradiction to the criteria used in the literature³³ for judging the variational quality of a band calculation according to the lowering of the band eigenvalues.

C. Total ground state-crystal energy

Our approach for calculating the total crystal energy is based on a direct use of Eq. (2). We have previously described¹³ how the various terms in this equation can be grouped so that the divergencies in the individual electron-electron and electron-nuclear energies per unit cell are cancelled. We have also shown how the kinetic and Coulomb terms are combined before their integration is attempted so as to affect a substantial numerical cancellation. We are able to obtain sufficient accuracy in the core eigenvalues by using some 10–30 Diophantine integration points inside the nuclear volume and about 300 integration points in the 1s orbital sphere. Table IV describes the results obtained with various local density models for diamond at the convergence limit of the SC cycle.

Basis set effects were seen to be significantly reduced in the limit of self-consistency relative to the noniterated results: while in the non-SC

TABLE III. Band structure of diamond at the high-symmetry Γ , X , and L points, obtained at the convergence limit of the SC exchange and correlation model. Values are given in eV relative to the bottom of the valence band ($\epsilon_{\Gamma_{1b}} = -30.94$ eV). The two core bands lie at 271.087 eV below vacuum. $\Delta_{\min,c}$ denotes the eigenvalue at the bottom of the conduction band. v and c denote valence and conduction, respectively.

| Γ point | | X point | | L point | |
|-----------------|--------|-------------------|--------|-----------|--------|
| Γ_{1b} | 0.0 | X_{1b} | 8.267 | $L_{2'v}$ | 5.271 |
| Γ_{25v} | 20.437 | X_{4v} | 14.346 | $L_{1'v}$ | 8.256 |
| Γ_{15c} | 26.771 | $\Delta_{\min,c}$ | 25.888 | L_{3v} | 17.617 |
| $\Gamma_{2',c}$ | 34.510 | X_{1c} | 29.041 | L_{3c} | 30.824 |
| | | X_{4c} | 37.129 | L_{1c} | 30.943 |
| | | | | L_{2c} | 38.957 |

limit the ion-pair basis (set II) yields a lowering of 1.43 eV/atom relative to set I, the difference in the SC limit is reduced to 0.4 eV/atom. Both the extended numerical set and the ion-pair set produce results that agree to within 0.4 eV (while a minimal numerical basis set yields a total energy that is about 1.7 eV higher). It would thus seem that the values obtained here with the ion-pair basis (set II) are probably close to the basis set convergence limit of our local density model.

The exchange and correlation energies ΔE_x and ΔE_{corr} (defined here as the corresponding *total energy* differences between the results obtained in independent SC calculations) form about 12 and 1%, respectively, of the total crystal energy and somewhat smaller fractions of the atomic total energy. It is rather difficult to estimate the correlation energy from other sources. One can obtain an estimate of the atomic “experimental” correlation energy from the work of Clementi⁵⁴ in which ΔE_{corr} is defined as the dif-

TABLE IV. Total (self-consistent) ground-state energies per carbon atom (values in eV). ΔE_x and ΔE_{corr} are defined as the difference in total energies between column 1 and 2 and 2 and 3, respectively. Lattice constant: 6.7403 a.u. The values in parenthesis indicate the virial ratio $-2T/V$.

| | Electrostatic model | Exchange model | Exchange and correlation model | ΔE_x | ΔE_{corr} |
|-------------------------------------|---------------------|----------------------|--------------------------------|--------------|--------------------------|
| Free atom ^a | -895.76 | -1008.23 [1.0002] | -1015.72 | 112.47 | 7.49 |
| Crystal extended set (set I) | -887.49 | -1015.10 [1.0036] | -1027.24 | 127.61 | 12.14 |
| Crystal ion-pair basis set (set II) | ... | -1015.52 [1.0004] | -1027.64 | ... | 12.12 |

^a Values obtained from a non-spin-polarized numerical SC calculation.

ference between the experimental total energy (with relativistic effects removed) and the best analytic Hartree-Fock energy. This yields some 4.3 eV for carbon in its 3P ground state. A somewhat smaller value can be deduced by comparing the total energies obtained from a configuration-interaction and a single-configuration Hartree-Fock (HF) study for carbon.⁵⁵ Our estimate of the atomic correlation energy is larger than the "experimental" values by a factor of 1.75; this discrepancy probably reflects the inadequacy of an electron-liquid correlation model for describing the discrete atomic excitation spectrum.⁵⁶ Similar results have been obtained previously by Tong and Sham⁴ and Kelly⁵⁷ using an interpolated Wigner⁵⁸ and Gell-Mann-Bruckner⁵⁹ correlation functional (although their results predict somewhat poorer agreement with experiment using the older correlation functions). Clearly, the local density functional is inadequate for estimating correlation energies in finite systems. Only crude estimates of the crystal correlation energy are possible. Comparison of HF and configuration-interaction calculations of the C_2 molecule⁶⁰⁻⁶² indicates a correlation energy of ~ 5.64 eV/atom. Taking the increase over the atomic correlation energy as an approximation to the carbon-bond correlation enhancement, one obtains a rough estimate of ≈ 10 eV/atom for the crystal correlation. A limited Heitler-London type configuration-interaction calculation on diamond indicates a stabilization by 21 ± 8 eV of the correlated state over the uncorrelated state.^{63,64} It would thus seem that our estimate for the crystal correlation energy (~ 12 eV) constitutes a substantial improvement over the atomic value. We note that the correlation energy calculated as a difference between the total energies of the separate SC exchange and correlation model and the exchange model is some 40% higher than that estimated from

$$\int V_{\text{corr}}(\rho_0(\vec{r}))\rho_0(\vec{r})d\vec{r},$$

where $\rho_0(\vec{r})$ is the density calculated from an *uncorrelated model* (i.e., lowest-order perturbative correction). This would indicate that higher-order effects brought about by the changes in charge density due to the incorporation of correlation effects in the *potential* (see Fig. 2) are as important as the direct first-order correlation energy term. Thus, inclusion of correlation corrections in a solid as simple additive terms to the uncorrelated total energy^{49,65} are bound to significantly underestimate the SC value. On the other hand, the crystal exchange energy calculated as a total energy difference (column 5 in Table V) is lower than that calculated by integrating

$$\frac{3}{4} \int V_x(\rho_0(\vec{r}))\rho_0 d\vec{r},$$

where $V_x(\rho_0(\vec{r}))$ is the exchange potential.

So far, correlation corrected HF total energy calculations on solids have not been published. A restricted HF calculation using an s and p Gaussian basis set yields a total crystal ground-state energy between²⁵ -1027.09 and²² -1030.39 eV. These values are in closer agreement with our best correlated value for the crystal than is the HF atomic total energy (-1025.507 eV) compared with our atomic LDF result.

The accuracy of any calculation of the cohesive energy is limited by the difficulty in determining both the atomic and the crystal total energies to the same level of approximation. Since the LDF formalism seems to overestimate the correlation energy in finite systems having no continuum of low-lying excited states, it is difficult to assess the validity of the atomic total energy calculation. In addition, spin polarization is expected to lower substantially the atomic total energy of an open-shell system like carbon relative to our spin-restricted calculation. Although spin-dependent electron-liquid correlation functionals are available,^{3,66} it is difficult to estimate the reliability of a cohesive energy calculation based on the use of different functionals for the atom and the solid. Our exchange model predicts in the non-spin-polarized atomic limit a cohesive energy of 7.29 eV while the exchange and correlation model predicts in the same limit a cohesive energy of 11.92 eV/atom. The experimental static binding energy of diamond (calculated by adding a Debye-model zero-point energy to the measured value¹⁶ using $\theta_D = 2230$ °K) is 7.62 eV/atom. Previous studies⁶⁷ have indicated that spin-polarization corrections to the atom tend to cancel the correlation enhancement of the crystal cohesive energy so that the result obtained from a non-spin-polarized exchange model comes very close to the accurate prediction. We have been informed by the referee of this paper: "I have a number for the ground-state energy of the free carbon atom, calculated with the spin-polarized exchange and correlation potential of Ref. 3 for the configuration

$$(1s\alpha)'(1s\beta)'(2s\alpha)'(2s\beta)'(2p\alpha)^2: -1021.9 \text{ eV},$$

which would give a cohesive energy of diamond equal to 5.7 eV, much closer to the experimental result. It should be stressed, however, that the interpolation formulas of Refs. 3 and 39 differ slightly at $r_s < 1$, i.e., in the core region."

The restricted HF value for the cohesive energy (with correlation and spin polarization neglected) is substantially lower (~ 5.2 eV/atom.)^{22,23} This is in line with the usual tendency of restricted

HF calculations to underestimate the binding energy relative to the correlated limit (e.g., 0.78 eV/atom is obtained for the binding of the C_2 molecule in the RHF level⁶¹⁻⁶² while 5.4–6.7 eV/atom are obtained in a CI calculation.⁶⁰ The experimental result is 6.36 eV/atom⁶⁸ compared with a local-exchange result of 5.58 eV/atom⁶⁹). We note that in our model correlation acts to stabilize the crystal over the atom by about 4.6 eV. An electrostatic-type calculation for diamond (column 2 in Table IV) seems to produce no binding at all.

Several calculations have been published previously on the cohesive energy of diamond. These include the t -matrix pseudopotential calculation of Bennemann,⁴⁹ the OPW pseudopotential calculation of Goroff and Kleinman⁶⁵ and the Heitler-London calculation of Schmidt⁶³ and Dermit.⁶⁴ We note that whereas Gorff and Kleinman have used a small-basis OPW calculation, a later extended basis OPW calculation³⁰ indicated very poor convergence of the eigenvalues containing p -like states before several thousands of OPW's are included. The correlation energy used both by Bennemann and by Goroff and Kleinman was treated as an additive term to the total energy without attempting to incorporate it self-consistently into the effective potential. The core-overlap contribution was also neglected in these studies. The calculation of Schmidt⁶³ based on an elegant and rigorous formulation of the Heitler-London model in an orthogonalized representation, involves extensive approximations in the practical evaluation of the LCAO integrals, resulting in large uncertainties in the cohesive energy.

In order to examine the prediction of the LDF formalism for the equilibrium lattice constant, we have repeated our total energy calculation using our extended numerical basis (set II) at seven unit-cell parameters. Such a calculation is free from the limitations of the cohesive energy problem in that only crystal results are considered. Using the SC results corresponding to the calculation with the closest lattice constant, only a few iterations of "state 2" in SC were required for each lattice constant. The resulting total energy curve was interpolated to yield the equilibrium lattice constant values of $a_{\text{eq}} = 3.662 \text{ \AA}$ for the exchange model and $a_{\text{eq}} = 3.581 \text{ \AA}$ for the exchange and correlation model. The fitting error in each of these cases is estimated to be 0.003 \AA . The experimental value is 3.567 \AA .¹⁷

These results are consistent with our previous conclusion that correlation acts to stabilize the crystal, increasing its binding energy and reducing the lattice constant. Similar good agreement with the experimental lattice constant

($a_{\text{calc}}/a_{\text{expt}} \sim 0.996-1.003$) was obtained in the OPW model of Goroff and Kleinman,⁶⁵ however, the approximations made in their work make it difficult to assess the accuracy of this result. The restricted HF value for a_{eq} is 3.545 \AA .²³ It is expected that correlation corrections would act to further reduce the HF value which is already somewhat smaller than experiment. Previous local-density SC non-muffin-tin exchange model calculations on simple molecules like C_2 ,⁶⁹ N_2 , CO , and H_2O ,⁴⁵ and LiF , NO , O_2 , and N_2 ,^{70, 71} seem to predict equilibrium bond lengths that are larger than experiment. Tong's¹² self-consistent cellular calculation on solid Na leads to the same conclusion. Calculations within the muffin-tin approximation^{7, 9} do not seem to reveal any systematic behavior of the deviations from experiment of the computed lattice constants. In view of the large non-muffin-tin corrections found⁶⁹ for the cohesive energy of some covalently bonded molecules,⁷² it seems rather unlikely that such calculations would lead to reliable results for solids like diamond.

D. Behavior of one-electron properties with change in lattice constant

In order to further elucidate the bonding mechanism in diamond, we have studied the changes in crystal charge density with lattice constant. Figure 8 reveals the charge-density changes in some high-symmetry states in the occupied portion of the BZ as a function of lattice constant. Upon decreasing the lattice constant from a value larger than the equilibrium value, charge density is shifted towards the bond region and simultaneously the density at the core region is *increased* (at the expense of depleting charge from an intermediate region).

This result confirms our earlier suggestion (cf. Figs. 1–3) that the bonding mechanism in diamond involves a stabilization of the crystal due to both a build up of charge density in the bond region (mainly due to exchange and correlation effects) and close to the core regions (due to penetration of neighboring wave functions). Both of these effects tend to decrease the positive kinetic energy, produced by the orthogonalization of the (overlapping) noninteracting atomic Bloch states, by enhancing the interaction with the attractive electron-nuclear, exchange, and correlation potentials. A minimal-basis-set description of diamond tends to remove charge from the core regions into the bond region thereby producing rather realistic values for the low-angle scattering factors (indicating a correct charge build-up in the bond region), but still yielding small val-

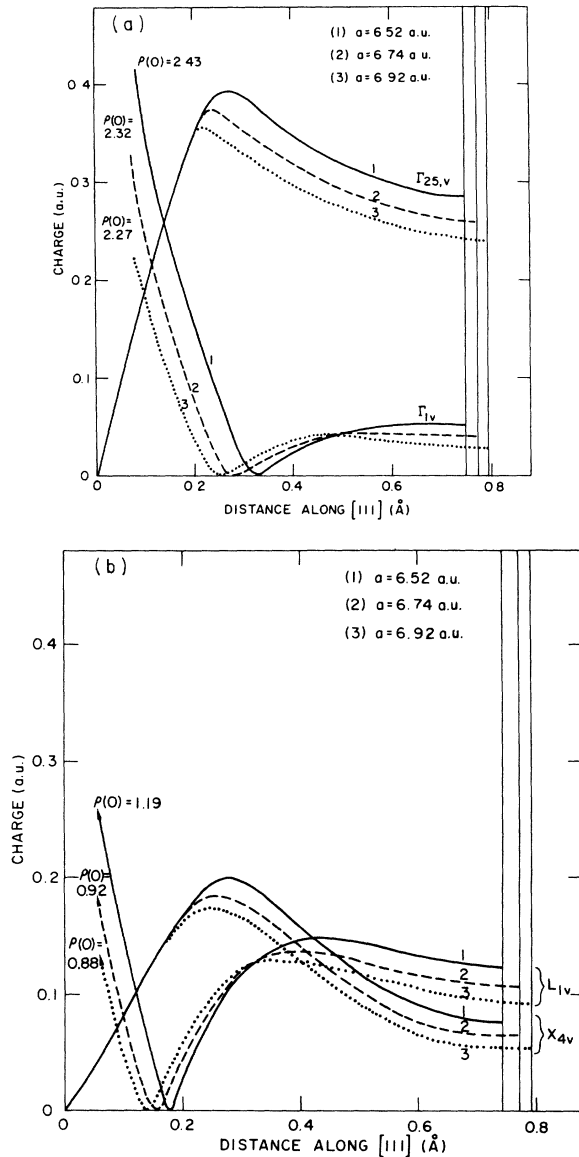


FIG. 8. Variation in the valence charge-density contributed by some high-symmetry states, with lattice constant, along the [111] direction in diamond. The two lowest $1s$ -like bands are not included in each case. An atom is placed at the origin (the three origins corresponding to the three lattice constants considered are denoted as 1, 2, 3) while the right-hand end of the x axis denotes the center of the C-C bond. (a) Γ point; (b) L and X points.

ues of the binding energy. Augmenting the set by additional orbitals with extended tails tends to restore the charge localization near the core, and thus produces an increase in the potential attraction in this region. It is the detailed balance between these two charge redistribution mechanisms that seems to yield the correct binding in

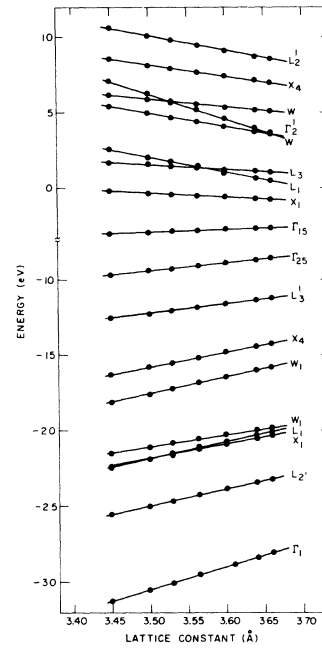


FIG. 9. Variation of one-electron energies in diamond with lattice constant. The full dots correspond to actually calculated points and smooth lines were fitted in between.

the solid.

Figure 9 shows the variation of the one-electron energies with lattice constant. As expected, the eigenvalues corresponding to the "bonding" occupied states are stabilized while the "non-bonding" and "antibonding" virtual states are mostly destabilized by compressing the lattice. There seems to be a striking linearity in the lattice-constant dependence in the range studied here, resulting in only a slight increase in the valence bandwidth upon contracting the lattice. It is interesting to observe that the conduction states at L_1 and L_3 interchange their order with change of lattice constant, the crossover being close to the experimental zero-pressure equilibrium value. Indeed, various band calculations reveal a marked sensitivity in the order of these levels to the details of the computational parameters. Thus, muffin-tin (APW²⁶ and LCAO³³) calculations produce $\epsilon_{L_1} < \epsilon_{L_3}$, while non-muffin-tin (OPW²⁹ and LCAO³³) calculations produce the reverse order. The photoelectric threshold ($-\epsilon_{\Gamma_{25}}$) increases with applied pressure by about 1.2 eV in the range shown in Fig. 9, while the bandwidth increases by 1.0 eV.

In order to compare the lattice constant behavior of the energy bands, we compute the pressure coefficient

$$\frac{d\epsilon_j(\vec{k})}{dp} = -K \frac{d\epsilon_j(\vec{k})}{d \ln V}, \quad (13)$$

where p is the pressure, K is the volume compressibility (0.18×10^{-12} dyn/cm² in diamond⁷³) and V is the unit-cell volume. Inspection of Fig. 9 indicates that the one-electron energy levels can be divided into distinct groups according to their pressure coefficients. In the valence band, the states near the bottom of the band having predominantly 2s character (e.g., $\Gamma_{1v}, X_{1v}, L'_{2v}$, etc.) have a rather large pressure coefficient [$(3-5) \times 10^{-6}$ eV/bar] while those near the top of the valence band are characterized by lower pressure coefficients (1.2×10^{-6} eV/bar for Γ_{25v} and 1.6×10^{-6} eV/bar for L'_{3v}). In the conduction bands, most states possess an antibonding character and have a large pressure coefficient [$(4-7) \times 10^{-6}$ eV/bar]. The nonbonding conduction states however have a very low coefficient (e.g., 0.32×10^{-6} eV/bar for X_{1c} , 0.78×10^{-6} eV/bar for L_{3c}). Transitions from the upper valence band to the low-lying nonbonding conduction state (e.g., $\Gamma_{25v} - X_{1c}$) would thus have a vanishingly small pressure coefficient while zone-center transitions ($\Gamma_{25v} - \Gamma_{1c}$) are predicted to have much higher (factor of $\sim 5-8$) pressure coefficients. Experimental data⁷⁴⁻⁷⁵ indeed seem to suggest an anomalously low-pressure coefficient for the $\Gamma_{25v} - X_{1c}$ transition. A similar study of the lattice-constant dependence of the band structure was performed at the restricted HF level by Surratt *et al.*²³ However, owing to an error in this study,⁷⁶ we are unable to compare our results directly with their data.

The variation in the (hkl) scattering reflections with lattice constant is depicted in Fig. 10. It is seen that when we change from an atomic superposition model (horizontal lines on the right) to a full crystalline description, the low-angle scattering factors increase substantially (in absolute value) and ultimately start decreasing when the solid is compressed. The high (hkl) reflections are rather insensitive to lattice constant variation, as expected. Interestingly, the (331) and (400) scattering factors change their relative order in going from an atomic superposition model ($f_{331} < f_{400}$) to the crystalline model ($f_{331} > f_{440}$). Solid-state effects introduced by wave-function overlap (as opposed to spherical charge-density overlap) are thus seen to be non-negligible.

E. Directional Compton profile

Although the LDF formalism makes no definite predictions on observables that depend on the individual eigenfunctions of the one-particle equation solved here (since they are not actual one-

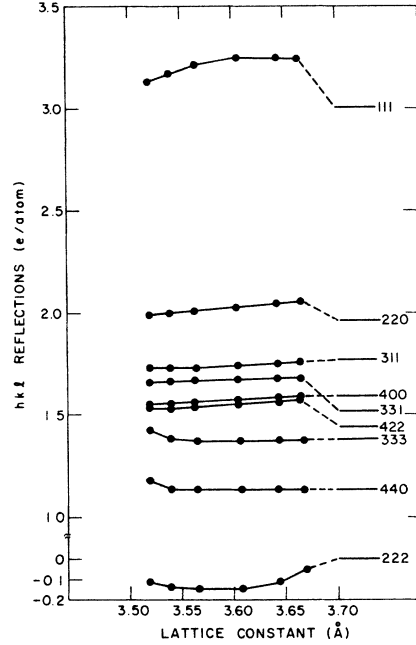


FIG. 10. Dependence of the x-ray scattering factors in diamond on the lattice constant. The straight lines on the right-hand side denote the atomic scattering factors as calculated by an atomic superposition exchange and correlation model.

particle states), its resemblance to an “effective” Hartree-Fock type equation makes it interesting to examine the quality of these wave functions as “pseudo”-one-particle states. Such a test is naturally provided by comparing the calculated directional Compton profile with experiment. We will thus assume⁷⁷ that the momentum density $\rho(\vec{p})$ can be represented by the sum of squares of the momentum eigenfunctions⁷⁸

$$\psi_j(\vec{p}) = \sum_{\mu=1}^n \sum_{\alpha=1}^h C_{\mu\alpha j}(\vec{k}) \Phi_{\mu\alpha}(\vec{p}), \quad (14)$$

where the Fourier-transformed Bloch function $\Phi_{\mu\alpha}(\vec{p})$ is obtained by direct three-dimensional Diophantine integration of

$$\Phi_{\mu\alpha}(\vec{p}) = \frac{1}{(2\pi)^{3/2}} \int e^{-i\vec{p}\cdot\vec{r}} \Phi_{\mu\alpha}(\vec{k}, \vec{r}) d\vec{r}. \quad (15)$$

Since each momentum value \vec{p} relates a point \vec{k}_i in the BZ with a given reciprocal lattice vector $\vec{G}_i = \vec{p}_i - \vec{k}_i$, we compute the crystal wave functions $\psi_j(\vec{k}, \vec{r})$ at a given grid $\{\vec{k}_i\}$ in the BZ and use these functions to obtain the momentum eigenfunctions $\psi_j(\vec{p})$ at a set of momentum points $\vec{p}_i = \vec{k}_i + \vec{G}_i$. In all, 52 \vec{k}_i inequivalent points are used to obtain the momentum density

$$\rho(\vec{p}) = \sum_j^{\text{occ}} n_j \psi_j^*(\vec{p}) \psi_j(\vec{p}) \quad (16)$$

for $p \leq 8$ a.u. This function is then interpolated by a fifth-order local interpolation to obtain $\rho(\vec{p})$ for arbitrary momentum and is then least-squares fitted to a Kubic harmonic expansion⁷⁹

$$\rho(\vec{p}) = \sum_{l,m}^{l_{\max}} a_{lm}(p) Y_{lm}(\hat{p}) \quad (17)$$

for $l_{\max} \leq 12$. The Compton profile $S(\vec{k}, \omega)$ in the impulse approximation is given by

$$\begin{aligned} S(k, \omega) &= \int \rho(\vec{p}) \delta\left(\omega - \frac{k^2}{2m} - \frac{\vec{k} \cdot \vec{p}}{m}\right) d\vec{p} \\ &= \frac{1}{k} S(\vec{q}, \hat{k}), \end{aligned} \quad (18)$$

where $\vec{q} = \hat{k} \cdot \vec{p}/m$. Expressing the reduced profile $S(\vec{q}, \hat{k})$ in a harmonic expansion as

$$S(\vec{q}, \hat{k}) = \sum_{l,m} S_{lm}(q) Y_{lm}(\hat{k}), \quad (19)$$

we obtain the expansion coefficients $S_{lm}(q)$ by a direct radial integration:

$$S_{lm}(q) = 2\pi \int_{|q|}^{\infty} p a_{lm}(p) P_l\left(\frac{q}{p}\right) dp, \quad (20)$$

where $P_l(q/p)$ is the Legendre polynomial. The Compton profiles in an arbitrary direction are obtained using Eqs. (19) and (20).

We give in Fig. 11 our calculated Compton profile differences for the [100]-[110] and [100]-[111] directions together with the experimental results and those yielded by the restricted HF model of Wepfer *et al.*²⁴ Table V gives our calculated results for the [100] direction together with the experimental results of Reed and Eisenberger²⁰ and Weiss and Phillips²¹ and for comparison, the calculated results of Seth⁸⁰ in the non-SC local-exchange model (with exchange coefficient of 0.70) and the restricted HF results of Wepfer *et al.*²⁴

The main conclusions to be drawn from this comparison are: (i) While the RHF results for the profile lack sufficient high-momentum components (and hence produce too high a profile at low-momentum transfer), our model predicts a slight excess of high-momentum components. The non-self-consistent exchange model⁸⁰ tends to produce a profile that is even higher than the RHF profile at low \vec{q} . This result is in line with previous calculations on atomic Compton profiles using the exchange model^{81,82} and with our results for a non-SC superposition model.¹⁴ We thus conclude that both the inclusion of correlation and the iteration towards self-consistency tend to redistribute the charge so as to add some high-momentum components to it. It was previously suggested that the same effect can be achieved (in atomic systems)

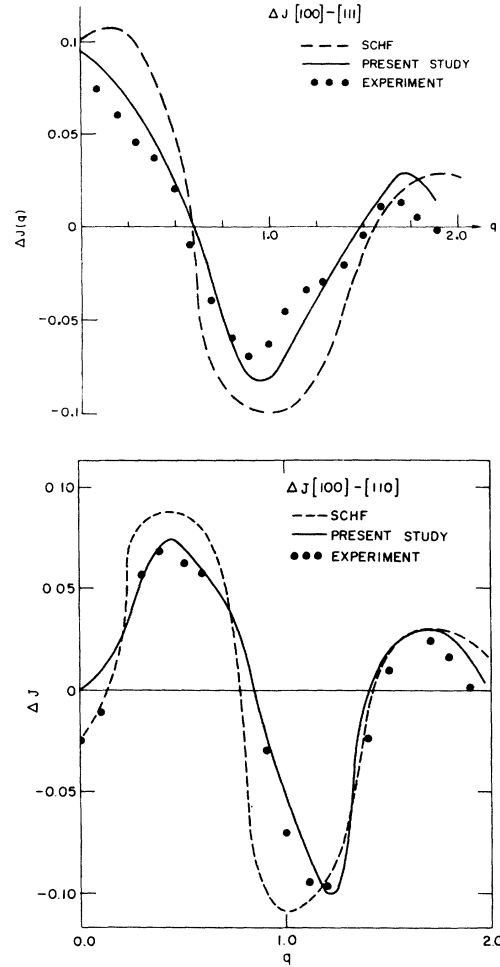


FIG. 11. Directional Compton profile in diamond as obtained from the self-consistent exchange and correlation model. (a) $\Delta J[100]-[111]$; (b) $\Delta J[100]-[110]$.

by either artificially increasing the exchange parameter or by adding a local correlation functional to the exchange potential.⁸² Previous superposition-model calculations for Si similarly indicate an overestimation of the low-momentum profile in this non-SC limit.⁸³ Iteration towards self-consistency also tends to increase the low-angle scattering factors¹⁴ (and hence to produce charge localization in the bond region) in accordance with its effect on the Compton profile. The occurrence of rather strong high momentum components in our results partially reflects some enhanced localization of the wave functions near the core regions (owing to nearest-neighbor penetration) relative to the exchange model and superposition limit¹⁴ (see also discussion in Sec. III A). (ii) While the RHF results agree with both experiment and with

TABLE V. Compton profile in diamond along the [100] direction.

| Momentum (a.u.) | SC | | Expt. ^b | SC HF model ^c |
|--------------------|--|--------------------------------------|--------------------|--------------------------------|
| | Non-SC exchange model ^a | exchange and correlation model | | |
| 0.0 | 2.230 | 2.05 | 2.09, 2.08 | 2.180 |
| 0.4 | 2.075 | 1.93 | 1.91, 1.94 | 2.046 |
| 0.8 | 1.575 | 1.52 | 1.46, 1.55 | 1.548 |
| 1.2 | 0.890 | 0.96 | 0.86, 0.94 | 0.884 |
| 1.6 | 0.455 | 0.48 | 0.47, 0.45 | 0.460 |
| 2.0 | 0.300 | 0.33 | ... 0.31 | 0.293 |
| 4.0 | 0.080 | 0.11 | ... 0.10 | ... |

^a Non-SC results of Seth (Ref. 80) using an exchange coefficient of 0.70 and a double-zeta Slater basis set.

^b The first value refers to the experimental results of Reed and Eisenberger (Ref. 20) while the second number gives the data of Weiss and Phillips (Ref. 21).

^c Reference 24.

our results for the anisotropy along [100]-[110] [Fig. 11(b)], the RHF directional profile for [100]-[111] is considerably more anisotropic than experiment and our data. We found that upon iterating our results to self-consistency (varying our basis set nonlinearly so as to allow more variational participation of the virtual 3s and 3p atomic orbitals into the valence band) the calculated anisotropy decreased. It would thus seem that by allowing the formerly virtual states (having long-range tails) to participate in the bonding manifold, the localization of the valence-band states decreases and a broader $\Delta J(\vec{q})$ is produced (along with an increase in the binding energy—as discussed in Sec. III C). It is possible that incorporation of such “plane wave” character would also diminish the anisotropy in the RHF profile.

The over-all agreement of our calculated Compton profile with experiment seems reasonable. It would thus seem that at least for diamond, the apparent anomaly [i.e., $J(\vec{q})$ too high at low q] of the calculated Compton profile in the exchange model for atoms (with an exchange coefficient of $\frac{2}{3}$) disappears in a SC exchange and correlation model. In such a covalently bonded system high-momentum components are added due to correlation, localization of charge in the core regions, and enhancement of the charge buildup in the bond center.

IV. SUMMARY

We have presented results obtained by applying a self-consistent numerical basis set LCAO treatment to the description of some ground-state

electronic properties of diamond in the LDF formalism. Our study of the effects of exchange and correlation on the ground-state charge density indicated that these act to increase the charge localization both in the “bond” region and to some extent close to the core region—correlation effects being much smaller than the exchange effects, although still considerably \vec{k} dependent and anisotropic. The x-ray scattering factors obtained from the SC charge density agree quite well with experiment and seem to account for the observed “forbidden” (222) reflection. Our calculated Compton profile similarly indicates good agreement with experiment; the deficiency in the LDF formalism in describing the atomic profile is remedied in the solid due to correlation and the above-mentioned charge redistribution effects.

Our total energy studies show a substantial increase in stability of the solid relative to the free atoms due to exchange and correlation although the latter is probably overestimated in the atom. The use of an ion-pair charge-transfer basis set is shown to be rather efficient in producing a converged LCAO expansion, in line with the previously established variational quality of the orthogonalized Heitler-London scheme for molecules.^{84,85} Our correlation model estimate for the cohesive energy in the non-spin-polarized atomic limit seems to overestimate the experimental value considerably. Since we are not able to assess the magnitude of the corrections required to account for the overestimation of the correlation in the atomic limit as well as the correct spin-polarization effects, this result is taken as a rough estimate only. Our exchange results for the cohesive energy in the non-spin-polarized atomic limit agree favorably with the experimental results and predict an equilibrium lattice constant that is about 3% too high. The full exchange and correlation model reduces the calculated lattice constant to within 0.5% of experiment. The HF model, on the other hand, seems to produce a lattice constant that is smaller than the experimental value even in the uncorrelated limit. Our study of the lattice-constant dependence of the band eigenvalues reveals an anomalously small pressure coefficient for the indirect $\Gamma_{25v} \rightarrow \Delta_{mt_{1u}c}$ transition together with a large pressure coefficient of the low-lying 2s-like valence states (but in opposite senses) and the conduction bands. All in all, it seems that the differences between the predictions of a HF nonlocal exchange model and a proper self-consistent LDF model for the ground state properties of diamond might be rather small compared with the differences induced by an improperly balanced basis set

expansion, muffin-tin approximations and lack of self-consistency. Further studies on other systems like BN, LiF, and TiS_2 are under way and will hopefully further elucidate the role of local versus nonlocal exchange in determining ground-state in properties of solids.

Note added in proof. We have been informed by Dr. O. Gunnarsson that a total energy calculation of the carbon atom in the spin-polarized local-spin density formalism (using the functional of Refs. 3 and 66) yields the value of -1019.83 eV. Using this value and our best result for the total energy

of the solid (-1027.64 eV/atom, Table IV), gives a binding energy of 7.81 eV/atom, which is in remarkable agreement with the observed value of 7.62 eV/atom. We are grateful to Dr. Gunnarsson for this communication.

ACKNOWLEDGMENT

The authors would like to acknowledge R. Euwema and E. Lafon for helpful discussions. We would like to thank A. Seth for making available his Compton routine and for helpful discussions.

*Supported by the NSF (DMR Grant Nos. 72-63101 and 72-03019) and the Air Force Office of Scientific Research (Grant No. 76-2948).

¹P. Hohenberg and W. Kohn, Phys. Rev. B **136**, 864 (1964).

²W. Kohn and L. J. Sham, Phys. Rev. **140**, A1133 (1965).

³O. Gunnarsson and B. I. Lundqvist, Phys. Rev. B **13**, 4274 (1976), and references therein.

⁴B. Y. Tong and L. J. Sham, Phys. Rev. **144**, 1 (1966).

⁵S. Lundqvist and C. W. Ufford, Phys. Rev. **139**, A1 (1965).

⁶O. Gunnarsson, P. Johansson, S. Lundqvist, and B. I. Lundqvist, Int. J. Quantum Chem. S **9**, 83 (1975).

⁷J. F. Janak, V. L. Moruzzi, and A. R. Williams, Phys. Rev. B **12**, 1757 (1975).

⁸E. C. Snow, Phys. Rev. B **8**, 5391 (1973).

⁹F. W. Averill, Phys. Rev. B **6**, 3637 (1972).

¹⁰N. D. Lang, Solid State Phys. **28**, 225 (1973).

¹¹J. R. Leite, B. I. Bennett, and F. Herman, Phys. Rev. B **12**, 1466 (1975).

¹²B. Y. Tong, Phys. Rev. B **6**, 1189 (1972).

¹³A. Zunger and A. J. Freeman, Int. J. Quantum Chem. S **10**, 383 (1976); this issue, Phys. Rev. B **15**, 4716 (1977).

¹⁴A. Zunger and A. J. Freeman, Phys. Lett. A **57**, 457 (1976).

¹⁵See for instance the review by G. S. Buberger, Usp. Fiz. Nauk. **103**, 675 (1971) [Sov. Phys. Usp. **14**, 180 (1972)].

¹⁶H. D. Hagstrum, Phys. Rev. **72**, 947 (1947); and in *JANAF Tables of Thermochemical Data*, edited by D. R. Stull (U.S. GPO, Midland, Michigan, 1965).

¹⁷J. Thewlis and A. R. Davey, Philos. Mag. **1**, 409 (1958).

¹⁸S. Göttlicher and E. Wölfel, Z. Elektrochem. **63**, 891 (1959).

¹⁹M. Renninger, Acta Crystallogr. **8**, 606 (1955).

²⁰S. A. Reed and P. Eisenberger, Phys. Rev. B **6**, 4596 (1972).

²¹R. J. Weiss and W. C. Phillips, Phys. Rev. **176**, 900 (1968).

²²R. N. Euwema, D. L. Wilhite, and G. T. Surratt, Phys. Rev. B **7**, 818 (1973).

²³G. T. Surratt, R. N. Euwema, and D. L. Wilhite, Phys. Rev. B **8**, 4019 (1973).

²⁴G. G. Wepfer, R. N. Euwema, G. T. Surratt, and D. L. Wilhite, Phys. Rev. B **9**, 2670 (1974).

²⁵R. N. Euwema and R. L. Greene, J. Chem. Phys. **62**,

4455 (1975).

²⁶R. Keown, Phys. Rev. **150**, 568 (1966).

²⁷J. R. P. Neto and L. G. Ferreira, J. Phys. C **6**, 3430 (1973).

²⁸F. Herman, Phys. Rev. **88**, 1710 (1957); **93**, 1714 (1954).

²⁹F. Bassani and M. Yoshimine, Phys. Rev. **130**, 20 (1963).

³⁰R. N. Euwema and D. J. Stukel, Phys. Rev. B **1**, 4692 (1970).

³¹L. Kleinman and J. C. Phillips, Phys. Rev. **125**, 819 (1962).

³²G. S. Painter, D. E. Ellis, and A. R. Lubinsky, Phys. Rev. B **4**, 3610 (1971).

³³R. C. Chaney, C. C. Lin, and E. E. Lafon, Phys. Rev. B **3**, 459 (1971).

³⁴P. W. Kervin and E. E. Lafon, J. Chem. Phys. **58**, 1535 (1973).

³⁵E. E. Lafon, M. I. T. Solid State and Molecular Theory Group Quarterly Progress Report No. 69, p. 66 (unpublished).

³⁶This is to say that extended basis sets do not change the band structure substantially and that the latter is also not very sensitive to the degree of self-consistency maintained, but that non-muffin-tin corrections as well as nonlocal pseudopotentials terms might have drastic effects on the results.

³⁷M. Rasolt and D. J. W. Geldart, Phys. Rev. Lett. **35**, 1234 (1975).

³⁸K. S. Singwi, A. Sjölander, P. M. Tosi, and R. J. Land, Phys. Rev. B **1**, 1044 (1970).

³⁹L. Hedin and B. I. Lundqvist, J. Phys. C **4**, 2064 (1971).

⁴⁰P. P. Ewald, Ann. Phys. (Leipzig) **64**, 253 (1921).

⁴¹C. B. Haselgrove, Math. Comput. **15**, 373 (1961).

⁴²Algorithm of D. J. Chadi and M. L. Cohen, Phys. Rev. B **8**, 5747 (1973); compare also Ref. 22.

⁴³K. H. Johnson and F. C. Smith, in *Computational Methods in Band Theory*, edited by P. M. Marcus, J. F. Janak, and A. R. Williams (Plenum, New York, 1971), pp. 377.

⁴⁴E. J. Baerends, D. E. Ellis, and P. Ros, Theor. Chim. Acta **27**, 339 (1972).

⁴⁵H. Sambe and R. H. Felton, J. Chem. Phys. **62**, 1122 (1975).

⁴⁶Similar effects in atoms were discussed in Ref. 4 and 5.

⁴⁷It is thus possible that the poor agreement obtained in

the HF (Refs. 23 and 25) calculation for that reflection does not reflect the nonlocal exchange effect but rather a basis set effect.

- ⁴⁸P. M. Raccah, R. N. Euwema, D. I. Stukel, and T. C. Collins, *Phys. Rev. B* **1**, 756 (1970).
⁴⁹K. H. Bennemann, *Phys. Rev.* **133**, A1045 (1964).
⁵⁰L. Kleinman and J. C. Phillips, *Phys. Rev.* **125**, 819 (1962).
⁵¹I. Goroff and L. Kleinman, *Phys. Rev.* **164**, 1100 (1967).
⁵²H. Clark, *Phys. Lett.* **11**, 41 (1964).
⁵³In view of this relative insensitivity of the Hamiltonian matrix elements to the details of the exchange and correlation at regions close to the nuclei, one might expect that the effects of gradient terms (Ref. 37) would likewise be largely offset by the large kinetic-energy terms at that region. The effects of the gradient terms at larger distances from the core are expected to be small due to the relative smoothness of the charge density in that region.
⁵⁴E. Clementi, *J. Chem. Phys.* **38**, 2248 (1963).
⁵⁵A. W. Weiss, *Phys. Rev.* **162**, 71 (1967).
⁵⁶B. Y. Tong, *Phys. Rev. A* **4**, 1375 (1971).
⁵⁷H. P. Kelly, *Phys. Rev.* **131**, 684 (1963).
⁵⁸E. Wigner, *Phys. Rev.* **46**, 1002 (1934).
⁵⁹M. Gell-Mann and K. Brueckner, *Phys. Rev.* **106**, 364 (1957).
⁶⁰P. F. Fougere and R. K. Nesbet, *J. Chem. Phys.* **44**, 785 (1966).
⁶¹R. J. Buenker, S. D. Peyerimhoff, and J. L. Whitten, *J. Chem. Phys.* **46**, 2029 (1967).
⁶²B. J. Bansil, *Rev. Mol. Phys.* **32**, 239 (1960).
⁶³L. A. Schmidt, *Phys. Rev.* **92**, 1373 (1953).
⁶⁴G. Dermit, *Phys. Rev.* **127**, 1110 (1962).
⁶⁵I. Goroff and L. Kleinman, *Phys. Rev. B* **1**, 2574 (1970).
⁶⁶O. Gunnarsson, B. I. Lundqvist, and S. Lundqvist, *Solid State Commun.* **11**, 149 (1971); U. von Barth and L. Hedin, *J. Phys. C* **5**, 1629 (1972).
⁶⁷O. Gunnarsson, B. I. Lundqvist, and J. W. Wilkins, *Phys. Rev. B* **10**, 1319 (1974).
⁶⁸E. A. Ballik and D. A. Ramsay, *Astrophys. J.* **137**, 84 (1963).
⁶⁹J. B. Danese, *J. Chem. Phys.* **61**, 3071 (1974).
⁷⁰E. J. Baerends and P. Ros, *Chem. Phys.* **2**, 52 (1973).
⁷¹E. J. Baerends, D. E. Ellis, and P. Ros, *Chem. Phys.* **2**, 41 (1973).
⁷²No binding at all is found in a muffin-tin calculation

for C₂, while a non-muffin-tin calculation was shown to yield a cohesive energy of 5.6 eV/atom (Ref. 69).

- ⁷³K. Geschneider, *Solid State Phys.* **16**, 275 (1964).
⁷⁴F. C. Champion and J. R. Prior, *Nature* **182**, 1079 (1958).
⁷⁵W. Paul, *J. Appl. Phys.* **32**, 2082 (1961).
⁷⁶Their published results indicate an apparently anomalous behavior in that both the valence and conduction bands (with the exception of the two low-lying Γ_{1v} and X_{1v} 2s-like states) *increase* in energy when the lattice constant decreases (viz., Fig. 2 and Table III in Ref. 23). Pressure-dependent optical experiments for some IV-IV compounds (Refs. 74 and 75) indicate clearly that the valence bands *decrease* in energy when pressure is applied. Again, we do not ascribe this anomaly to any serious defect in the Hartree-Fock method. It seems likely that the integration constant appearing in Surratt *et al.*'s procedure for evaluating the electrostatic potential as an Ewald summation of point charges (rather than the Gaussian charge density) was omitted from the calculation. This would affect the lattice constant dependence of the eigenvalues (the omitted integration constant being volume dependent) but would cancel out in the total energy calculation. We are grateful to Dr. R. N. Euwema for suggesting this explanation to us.
⁷⁷The correct momentum density in the LDF formalism is given by the sum of squares of the momentum eigenfunctions $\psi_j(\vec{p})$ (e.g., as in the HF model in which the eigenfunctions are well-defined single-particle states) plus an additional term representing the mutual dependence of the LDF eigenfunctions due to correlation coupling.
⁷⁸L. Lam and P. M. Platzman, *Phys. Rev. B* **9**, 5177 (1974).
⁷⁹P. E. Mijnarends, *Phys. Rev.* **160**, 512 (1967).
⁸⁰A. Seth, Ph.D. thesis (Northwestern University, 1975) (unpublished).
⁸¹R. N. Euwema and G. T. Surratt, *J. Phys. C* **7**, 3655 (1974).
⁸²J. R. Sabin and S. B. Trickey, *J. Phys. B* **8**, 7593 (1975).
⁸³W. Schulke and W. Lucht, *Phys. Status Solidi B* **59**, K107 (1973).
⁸⁴J. C. Slater, *J. Chem. Phys.* **19**, 2206 (1951).
⁸⁵A. C. Hurley, J. Lennard-Jones, and J. A. Pople, *Proc. R. Soc. A* **220**, 446 (1953).